

Predicting Charge Transport in the Presence of Polarons: The Beyond-Quasiparticle Regime in SrTiO₃

Jin-Jian Zhou¹ and Marco Bernardi^{1,*}

¹*Department of Applied Physics and Materials Science,
California Institute of Technology, Pasadena, CA 91125, USA.*

In materials with strong electron-phonon (e -ph) interactions, the electrons carry a phonon cloud during their motion, forming quasiparticles known as polarons. Predicting charge transport and its temperature dependence in the polaron regime remains an open challenge. Here, we present first-principles calculations of charge transport in a prototypical material with large polarons, SrTiO₃. Using a cumulant diagram-resummation technique that can capture the strong e -ph interactions, our calculations can accurately predict the experimental electron mobility in SrTiO₃ between 150–300 K. They further reveal that for increasing temperature the charge transport mechanism transitions from band-like conduction, in which the scattering of renormalized quasiparticles is dominant, to a beyond-quasiparticle transport regime governed by incoherent contributions due to the interactions between the electrons and their phonon cloud. Our work reveals long-sought microscopic details of charge transport in SrTiO₃, and provides a broadly applicable method for predicting charge transport in materials with strong e -ph interactions and polarons.

I. INTRODUCTION

Understanding charge transport in complex materials is a grand challenge of fundamental and technological relevance. The interactions between electrons and phonons (the quanta of lattice vibrations) set an intrinsic limit for the conductivity and typically control charge transport near room temperature. When electron-phonon (e -ph) interactions are weak, charge transport is well described by the scattering of quasiparticles (QPs) [1], leading to the well-known band-like conduction regime. As the e -ph interactions become stronger, the electrons are dressed by a cloud of phonons, forming composite charge carriers known as polarons [2–4]. In the limit of strong e -ph coupling, the electrons are self-trapped by the lattice distortions, and the conduction mechanism becomes the thermally activated hopping of localized polarons [5].

Many oxides and organic crystals exhibit e -ph coupling strengths intermediate between the band-like and polaron hopping limits. In this so-called “large polaron” regime, the charge transport mechanisms and their temperature dependence are not well understood. The transition from band-like to hopping conduction for increasing e -ph coupling strength is also unclear, and recent work on the Holstein model uncovered an incoherent transport regime at intermediate coupling [6]. Yet, predictive calculations and microscopic understanding of charge transport in the intermediate e -ph coupling regime remain an open challenge.

Strontium titanate (SrTiO₃), which is stable in the cubic phase above 105 K, is a prototypical material with intermediate e -ph coupling in which large polaron effects are clearly seen in experiments [7–10]. Charge transport in SrTiO₃ is a decades-old problem [11–16], yet its underlying microscopic mechanisms are still debated [17]. The

electron mobility in cubic SrTiO₃ exhibits a roughly T^{-3} temperature dependence above 150 K [15, 16], which is commonly attributed to the scattering of electron QPs with phonons [11–14]. Different phenomenological models based on QP scattering have been proposed that can fit the experimental transport data [13, 18]. However, the carrier mean free paths extracted from experiment in SrTiO₃ fall below the interatomic distance [16], violating the Mott-Ioffe-Regel (MIR) criterion for the applicability of the QP scattering picture [19]. While there is consensus that large polarons are present in SrTiO₃ [7–10, 20], charge transport in this regime cannot yet be predicted, and detailed microscopic understanding has remained elusive [17].

First-principles calculations based on lowest-order e -ph scattering plus the Boltzmann transport equation (BTE) [21] can accurately predict the conductivity in simple metals and semiconductors [22–26]. We have recently shown [27] that when this approach is applied to SrTiO₃, one can obtain an accurate temperature dependence for the electron mobility if all the phonons (including the soft modes) are taken into account. However, the absolute value of the computed electron mobility is an order of magnitude greater than experiment [27]. It is clear that QP scattering alone cannot explain charge transport in SrTiO₃, consistent with the MIR limit violation; a fully quantum mechanical framework is needed to predict charge transport in this beyond-QP regime.

Here we show first-principles calculations of charge transport in cubic SrTiO₃ using a finite-temperature retarded cumulant approach that includes higher-order e -ph interactions and goes beyond the QP scattering picture. Our calculations can accurately predict the experimental electron mobility in SrTiO₃ between 150–300 K, and further shed light on its microscopic origin. We show that the weight of the QP peak in the electron spectral function is strongly renormalized, with significant weight

* E-mail: bmarco@caltech.edu

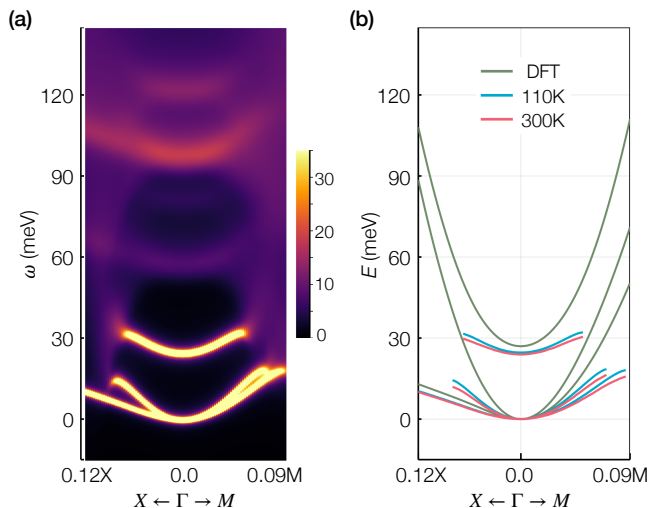


FIG. 1. (a) Combined spectral functions $A_{n\mathbf{k}}(\omega)$ for the three lowest conduction bands in cubic SrTiO₃, for \mathbf{k} along the Γ - X and Γ - M Brillouin zone directions at 110 K. (b) The energy-momentum dispersion of the QP peaks of the spectral function, shown at 110 K and 300 K, compared with the electronic band structure from DFT. The zero of the energy axis is set to the conduction band minimum.

transfer to the incoherent phonon satellites. While the renormalized QPs control transport at low temperature, the incoherent contributions from the phonon satellites and large momentum states are significant at room temperature, indicating a transport regime beyond the QP scattering paradigm. Consistent with these trends, our analysis shows that near room temperature the scattering rate (extracted from the optical conductivity) breaks the Planckian limit of $k_B T$ for semiclassical transport [28], clearly indicating a beyond-QP charge transport regime. Our work opens new avenues for computing charge transport in complex materials with large polarons and beyond the QP scattering regime.

II. ELECTRON SPECTRAL FUNCTION

Central to our approach for computing charge transport is the electron spectral function, $A(\omega)$, which can be seen as the density of states of a single electron. Due to the interactions with the phonons, the spectral function consists of a QP peak representing a single-electron-like excitation and an incoherent part including both phonon satellite peaks and a background contribution [29, 30]. While the spectral weights of the QP peak and incoherent part may vary, they always add up to one due to the sum rule $\int d\omega A(\omega) = 1$, which amounts to a conservation of the electron. To investigate the dynamics of the electrons and their interactions with the phonons, we compute the spectral function with a finite-temperature retarded cumulant approach that can account for higher-order e -ph interactions (see Appendix A), and use it di-

rectly to predict transport, without relying on QP scattering approaches.

We focus on the electron spectral function in cubic SrTiO₃ above 110 K. Leveraging our recently developed approach [27], which combines density functional theory (DFT), its linear response extension [31] and the temperature dependent effective potential (TDEP) method [32], we compute the band structure, lattice vibrations and e -ph interactions for all phonon modes, including the soft modes due to the lattice anharmonicity (see Appendix B). Using these quantities, we calculate the spectral function using a retarded cumulant formalism [33, 34]. In this framework, the e -ph interactions for each electronic state $|n\mathbf{k}\rangle$ with band index n and momentum \mathbf{k} are included in the one-particle retarded Green's function $G_{n\mathbf{k}}^R$ via the so-called cumulant function $C_{n\mathbf{k}}(t)$:

$$G_{n\mathbf{k}}^R(\omega) = -i \int_0^\infty e^{i(\omega - \varepsilon_{n\mathbf{k}})t} e^{C_{n\mathbf{k}}(t)} dt, \quad (1)$$

where $\varepsilon_{n\mathbf{k}}$ is the DFT band electron energy and $C_{n\mathbf{k}}(t)$ is obtained from the off-shell lowest-order e -ph self-energy, $\Sigma_{n\mathbf{k}}(\omega)$ [21], as

$$C_{n\mathbf{k}}(t) = \int_{-\infty}^\infty d\omega \frac{|\text{Im}\Sigma_{n\mathbf{k}}(\omega + \varepsilon_{n\mathbf{k}})|}{\pi\omega^2} (e^{-i\omega t} + i\omega t - 1). \quad (2)$$

The spectral function is then obtained from the retarded Green's function, using $A_{n\mathbf{k}}(\omega) = -\text{Im}G_{n\mathbf{k}}^R(\omega)/\pi$. Our finite-temperature retarded cumulant approach (see Appendix A) further allows us to compute the spectral function at various temperatures. This approach includes higher-order e -ph Feynman diagrams beyond the Migdal approximation [35], and it produces accurate spectral functions (see below) that can capture the strong e -ph interactions. On the other hand, we have verified that the lowest-order Dyson-Migdal approximation generates spectral functions with large errors in the QP spectral weight and satellite energies, consistent with recent results at zero temperature [36].

The computed electron spectral functions for the three lowest conduction bands in cubic SrTiO₃ at 110 K are combined in a color map and shown in Fig. 1(a). Each state exhibits a rather sharp QP peak at low energy and broader phonon satellite peaks at higher energies (~ 60 meV or more above the QP peak). By tracking the low-energy QP peaks, we map the energy-momentum dispersion of the QPs. Figure 1(b) shows that the interacting QPs exhibit a heavier effective mass than in the DFT band structure calculations, in which the e -ph interactions are not included. The mass enhancement is a factor of 1.8–2.6 for different bands and directions, and it increases only slightly with temperature. Taking the lowest bands along Γ - M as an example, the DFT effective mass is roughly $0.75m_e$ (m_e is the electron mass), compared to a QP effective mass of $1.4m_e$ at 110 K and a slightly heavier mass of $1.6m_e$ at 300 K. The mass enhancement is thus roughly a factor of 2, in excellent agreement with experimental results at light doping [7, 10].

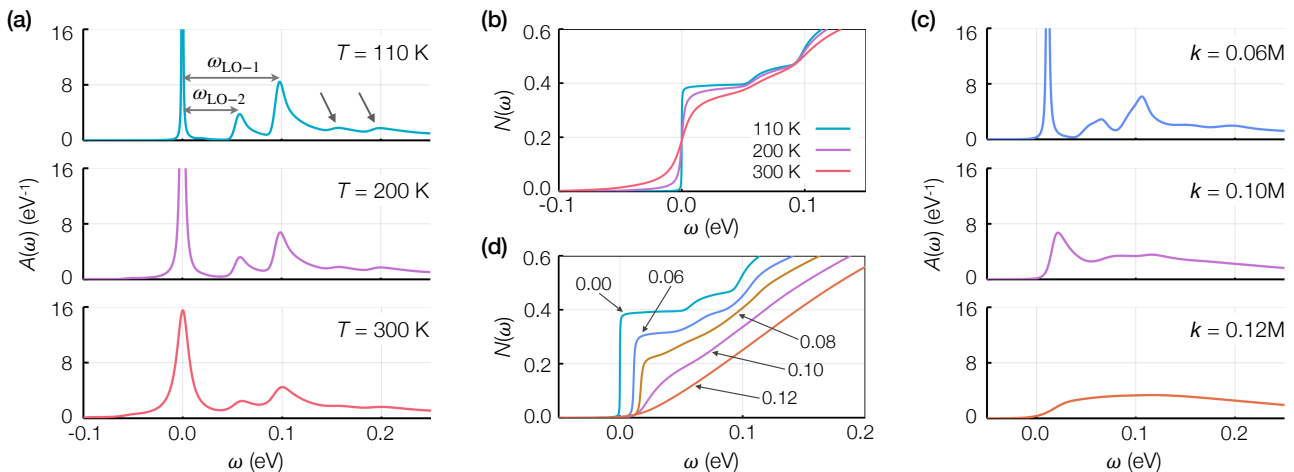


FIG. 2. Computed electron spectral functions $A_{\mathbf{k}}(\omega)$ for the lowest conduction band in cubic SrTiO₃. In each panel, the zero of the ω energy axis is set to the energy of the QP peak at the Γ point. (a) The spectral function $A_{\mathbf{k}}(\omega)$ at three temperatures between 110–300 K, for $\mathbf{k} = \Gamma$. The energies of the two LO phonons that couple strongly with the electrons are labelled $\omega_{\text{LO-1}}$ and $\omega_{\text{LO-2}}$, and the arrows point to the second set of satellites at $2\omega_{\text{LO-1}}$ and $\omega_{\text{LO-1}} + \omega_{\text{LO-2}}$. (b) The spectral weight $N(\omega)$ obtained by integrating the spectral function up to an energy ω . (c) The spectral function $A_{\mathbf{k}}(\omega)$ at 110 K for different values of \mathbf{k} along the Γ – M Brillouin zone line, and (d) The corresponding integrated spectral weight $N(\omega)$.

The interactions with the surrounding phonons not only make the electron QPs heavier, they also significantly reduce the QP spectral weight to a value well below one, transferring weight to the higher-energy incoherent phonon satellites. The QP peak even disappears at large electron momenta, leaving a spectral function made up entirely by the incoherent background. These trends are analyzed in detail below and in Fig. 2, focusing on how the spectral function of the lowest conduction band changes as a function of temperature and momentum.

The spectral function at the conduction band minimum at Γ exhibits a main QP peak, two main satellites (also known as phonon sidebands or replicas), and weaker additional satellites at higher energy [see Fig. 2(a)]. The two main satellite peaks are at an energy $\omega_{\text{LO-1}} = 98$ meV and $\omega_{\text{LO-2}} = 57$ meV above the main QP peak; these values correspond, respectively, to the energies of the two longitudinal optical (LO) modes with long-range e -ph interactions that exhibit the strongest coupling with electrons [27]. Note also the presence in Fig. 2(a) of weak phonon sideband peaks at energies of $2\omega_{\text{LO-1}}$ and $\omega_{\text{LO-1}} + \omega_{\text{LO-2}}$. These higher-order replicas, which are known to occur in the strong coupling limit of the Holstein model [37], are akin to the higher harmonics observed in phonon Floquet states [38]; they are a signature of strong coupling with the LO modes.

The main phonon sidebands are associated with the polaron plus one-phonon continuum, and are a hallmark of the large polaron regime [39]. Note that our calculations are performed on lightly n -doped SrTiO₃, with the chemical potential lying below the lowest QP peak; therefore, as expected, the phonon satellites appear at energy *higher* than the QP peak as they correspond to the excitation of an “electron-like” QP plus one LO

phonon [29, 36]. On the other hand, recent angle-resolved photoemission measurements on heavily n -doped samples, in which the chemical potential is above the QP peak, revealed a phonon sideband roughly ~ 100 meV *below* the QP peak, which corresponds to the excitation of a “hole-like” QP plus one LO phonon [9, 10, 29]. The energy difference between the QP peak and phonon sideband observed in experiments is in very good agreement with the $\omega_{\text{LO-1}} = 98$ meV energy difference between the QP peak and the most intense satellite peak found in our computed spectral function. We have verified that at high doping our approach also gives satellites with energies lower than the QP peak, consistent with experiment. The fact that the satellite position can be higher or lower than the QP peak depending on doping is well known [29, 40], but since inverse photoemission measurements are challenging, the low doping regime we compute here is rarely probed experimentally.

To compute the spectral weights of the QP peak and incoherent part, we integrate the spectral function up to an energy ω , obtaining the spectral weight $N(\omega) = \int_{-\infty}^{\omega} A(\omega') d\omega'$ given in Fig. 2(b). We find that the spectral weight of the QP peak is ~ 0.4 at 110 K, and thus much less than the unit value of the weak e -ph interaction limit. As the temperature increases from 110 K to 300 K, both the QP peak and the phonon satellites are broadened and smeared out [see Fig. 2(a)], but the QP spectral weight changes only slightly, primarily due to an overlap between the QP peak and the phonon satellites near 300 K. At all temperatures between 110–300 K, the QP weight is strongly renormalized to a value of ~ 0.4 , implying that (pictorially) only half of the electron resides in the QP state, while the other half contributes to the incoherent dynamical interactions with the phonons.

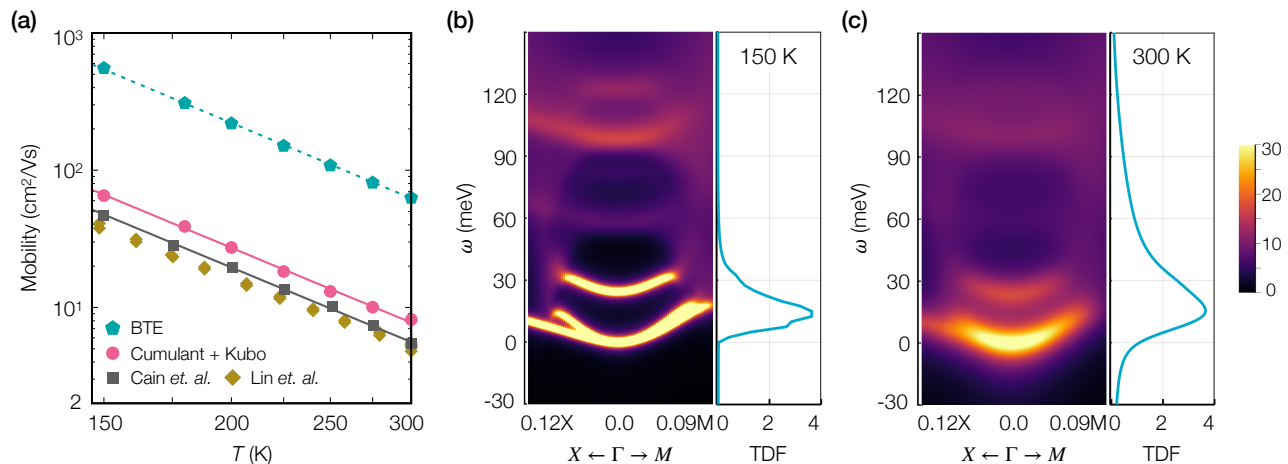


FIG. 3. (a) Electron mobility as a function of temperature, computed using the retarded cumulant approach plus the Kubo formula (red circles) and compared with experimental values taken from Refs. [15, 16]. The mobility computed in Ref. [27] using lowest-order e -ph scattering plus the BTE is also shown (blue pentagons). (b) The combined conduction-band spectral functions at $T = 150$ K are shown together with the TDF defined in Eq. (5), which quantifies the contribution to the DC conductivity as a function of electron energy ω . (c) The same quantities as in (b) shown at $T = 300$ K. The zero of the energy axis is set to the energy of the lowest QP peak.

Figure 2(c) reveals the disappearance of the QP peak at large enough momentum \mathbf{k} by showing how the spectral function changes as we increase \mathbf{k} along the Γ - M Brillouin zone line. We find that the QP spectral weight decreases with increasing momentum [see Fig. 2(d)] and that the QP peak ultimately disappears at $\mathbf{k} = 0.12M$, leading to a fully incoherent spectral function at larger momenta. These so-called end points of the QP peak, which have been predicted in both the Fröhlich [41] and Holstein models [42], are yet another signature of the strong e -ph interactions. The decrease of the QP spectral weight and the disappearance of the QP peak at large momentum have a significant impact on transport, as we discuss below.

III. ELECTRON MOBILITY

Large polaron transport is commonly believed to be the band-like conduction of QPs with enhanced effective mass. However, this simplified picture neglects the fact that the QP weight can drop to values much smaller than one (here, to roughly 0.4, as discussed above), and that the contribution to transport from the incoherent part of the spectral function can be significant. Temperature also plays a primary role. At low temperature, the electrons occupy the low-energy QP states, and there are only few LO phonons due to their relatively high energy. As the temperature increases, thermal fluctuations push the electrons to higher energies, exciting the electrons outside of the QP peak into the incoherent regime. In addition, the number of LO phonons grows rapidly with temperature, leading to strong dynamical interactions between the electron and its phonon cloud. The incoherent contributions are thus expected to significantly

influence transport at higher temperatures.

To investigate these points quantitatively in SrTiO₃, we compute the conductivity directly from the spectral functions – therefore including both the QP and incoherent contributions – using the Kubo formula [39]. In the absence of current-vertex corrections, the conductivity can be expressed as [43, 44]

$$\sigma_{\alpha\beta}(\omega) = \frac{\pi\hbar e^2}{V_{\text{uc}}} \int d\omega' \frac{f(\omega') - f(\omega' + \omega)}{\omega} \times \sum_{n\mathbf{k}} v_{n\mathbf{k}}^\alpha v_{n\mathbf{k}}^\beta A_{n\mathbf{k}}(\omega') A_{n\mathbf{k}}(\omega' + \omega), \quad (3)$$

where $\mathbf{v}_{n\mathbf{k}}$ is the band velocity of the electronic state $|n\mathbf{k}\rangle$, $f(\omega)$ is the Fermi-Dirac distribution, V_{uc} is the unit cell volume, and α and β are Cartesian directions. We also compute the DC conductivity, using $\sigma^{dc} = \sigma(\omega \rightarrow 0)$, and the electron mobility as $\mu = \sigma^{dc}/n_c e$, where the carrier concentration n_c is computed as

$$n_c = \sum_{n\mathbf{k}} \int_{-\infty}^{\infty} d\omega f(\omega) A_{n\mathbf{k}}(\omega). \quad (4)$$

We perform mobility calculations in the lightly doped regime, with electron concentrations ranging between 10^{17} – 10^{18} cm⁻³, and find that the computed mobility is nearly independent of the chosen concentration above 150 K, consistent with experimental data [15, 16].

Our computed electron mobility in SrTiO₃ as a function of temperature is shown in Fig. 3(a) and compared with experimental data taken from Refs. [15, 16]. Both the absolute value and the temperature dependence of the computed mobility are in excellent agreement with experiments. Our computed mobility at 300 K is about 8 cm²/Vs, versus an experimental value of ~ 5

cm^2/Vs [15, 16]. For comparison, the mobility obtained using lowest-order e -ph scattering plus the BTE is an order of magnitude higher than experiments [27], as also shown in Fig. 3(a).

The order-of-magnitude mobility drop from the BTE to the cumulant approach in SrTiO_3 is due to both the QP renormalization and the incoherent contributions. The cumulant approach clearly shows that the QP peak is strongly renormalized with significant weight transfer to higher energy incoherent satellites, and the QP peak even disappears as momentum \mathbf{k} goes beyond the end points [see Fig. 2 and Fig. 3(b,c)]. However, the BTE inherently assumes that the QP states are well defined for all bands and momentum values, so it fails to capture the contributions from the incoherent part of the spectral function, thus placing all the weight in the QP peak and significantly overestimating the mobility. Our results show unambiguously that the established lowest-order e -ph plus BTE approach [21–26] is accurate only in the case of weak e -ph interactions. Including higher-order e -ph processes and incoherent polaron effects via the cumulant approach greatly improves the computed mobility in materials with strong e -ph coupling.

Correctly taking into account the contributions from all the phonon modes, including the soft modes [27], is also essential for predicting the electron mobility and its temperature dependence in SrTiO_3 . Neglecting the soft mode in the calculations leads to significant errors in the computed mobility and its temperature dependence (see Fig. 5 in Appendix C), both in the BTE and in the cumulant approach. These results show that the soft modes, and not just the LO phonons as is widely believed, also contribute to charge transport in the large polaron regime.

Lastly, note also that in the weak e -ph coupling limit, in which the spectral function consists only of a sharp QP peak and no incoherent contributions, the expression we use for σ^{dc} reduces to the conductivity obtained from the relaxation time approximation (RTA) of the BTE [43, 45]. For a material with weak e -ph interactions and negligible polaron effects, one thus expects that the cumulant and BTE approaches predict the same transport results. We perform this sanity check for GaAs, showing that its mobility curves computed with the cumulant and BTE-RTA are in close agreement (see Fig. 6 in Appendix D). In the case of SrTiO_3 , on the other hand, it is apparent that the BTE cannot predict the mobility correctly.

IV. COHERENT AND INCOHERENT CONTRIBUTIONS

Our approach for computing the conductivity in the presence of polarons further allows us to resolve the coherent and incoherent contributions to transport and to uncover different transport regimes as a function of temperature. We write the DC conductivity as $\sigma^{dc} =$

$\int \Phi(\omega) d\omega$, where the integrand

$$\Phi(\omega) = \frac{\pi \hbar e^2}{V_{\text{uc}}} \sum_{n\mathbf{k}} v_{n\mathbf{k}}^\alpha v_{n\mathbf{k}}^\beta |A(n\mathbf{k}, \omega)|^2 \left(-\frac{\partial f(\omega)}{\partial \omega} \right), \quad (5)$$

is referred to as the transport distribution function (TDF), and is employed here to quantify the contributions to the DC conductivity as a function of electron energy ω . We analyze the TDF in the 150–300 K range in Fig. 3(b,c), and find that both the coherent QP peak and the incoherent part contribute to transport. At temperatures below ~ 200 K, the TDF spans primarily the QP peaks [see Fig. 3(b)], implying that transport is dominated by the scattering of QPs with a strongly renormalized spectral weight. As the temperature increases, the high-energy tail of the TDF extends over the incoherent contributions [see Fig. 3(c)], which become important and contribute by as much as 40% to the conductivity at 300 K, as discussed below. Therefore, transport near room temperature is governed not only by the weight-renormalized QPs, but also by the incoherent phonon satellites above the QP peaks and by the polaron states at large momenta beyond the end points, where the QP peaks disappear. The picture of QP scattering is in-

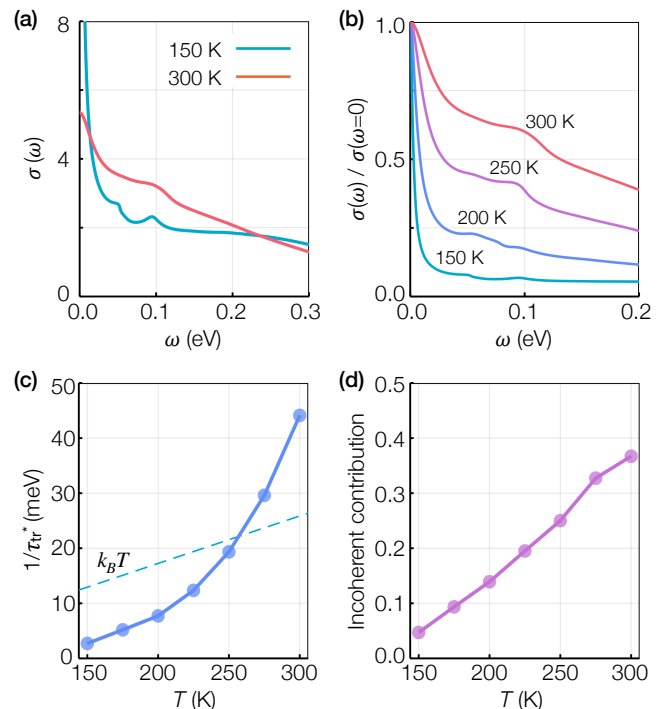


FIG. 4. (a) Comparison between the computed optical conductivities at 150 K and 300 K. The curves were normalized to possess the same integral. (b) Computed optical conductivity divided by the DC conductivity at each temperature. (c) The inverse of the effective transport relaxation time, τ_{tr}^{*-1} , extracted from $\sigma(\omega)$ and shown as a function of temperature. The Planckian limit $k_B T$ is shown with a dashed line. (d) The incoherent contribution to charge transport, quantified by the DC conductivity ratio $\sigma_{\text{inc}}^{dc}/\sigma^{dc}$ defined in the text.

adequate to describe transport at room temperature in SrTiO₃, and a more complex picture emerges in which transport is an interplay between the QP renormalization and the contributions from the incoherent phonon sidebands and from the polaron states beyond the end points, all of which are consequences of the dynamical interactions between the electrons and the phonon cloud.

These conclusions are supported by experiments on the optical conductivity. Recent experiments in SrTiO₃ show that the Drude peak at low frequency in the optical conductivity, which is associated with the coherent band-like transport of QPs, loses weight for increasing temperatures up to 300 K [7, 8]. Figure 4(a) compares the low-energy optical conductivities at 150 K and 300 K, both computed with Eq. (3) and normalized to possess the same integral, consistent with the optical sum rule. The optical conductivities exhibit a Drude-like peak centered at zero frequency, and an incoherent shoulder structure consisting of phonon sidebands plus a broad background. We find a significant weight transfer from the Drude peak to the incoherent shoulder as the temperature increases from 150 K to 300 K, in agreement with experiments [7]. The Drude peak is sharp at 150 K, but it broadens rapidly as the temperature increases [see Fig. 4(b)]. These trends confirm the transition seen in our transport results from a renormalized QP regime at low temperature to an incoherent, beyond-QP regime near room temperature.

We also extract an effective transport relaxation time, τ_{tr}^* , from the optical conductivity through the extended Drude analysis of Ref. [46]:

$$\tau_{\text{tr}}^* = -\frac{2}{\pi\sigma^{dc}} \int_0^\infty \frac{1}{\omega'} \frac{\partial\sigma(\omega')}{\partial\omega'} d\omega'. \quad (6)$$

Figure 4(c) shows the inverse of τ_{tr}^* , namely the effective scattering rate characterizing the width of the Drude peak. We find that this effective scattering rate increases rapidly with temperature, reaching values much greater than the QP scattering rate extracted from the QP peak of the spectral function in Fig. 2(a). Due to the uncertainty principle, in a semiclassical transport regime the scattering rate cannot exceed the so-called Planckian limit of $k_B T$ [28]. We find that the effective scattering rate in SrTiO₃ exceeds the Planckian limit $k_B T$ above 250 K, highlighting the beyond-quasiparticle nature of charge transport in SrTiO₃ near room temperature. The breaking of the Planckian limit in SrTiO₃ at room temperature is consistent with very recent results obtained by Mishchenko *et al.* using a model Hamiltonian [47].

Finally, one expects the incoherent contributions to transport to be significant at temperatures where the scattering rate exceeds the Planckian limit, namely above ~ 250 K in our calculations. We quantify the incoherent contribution to transport by defining the conductivity ratio $\sigma_{\text{inc}}^{dc}/\sigma^{dc}$, where the incoherent contribution to the conductivity σ_{inc}^{dc} is obtained by integrating the TDF at energies greater than all QP peaks ($\omega > 32$ meV in our calculations). Figure 2(d) shows that above 250 K the beyond-QP incoherent contributions amount to up

to $\sim 40\%$ of the total DC conductivity, confirming that the Planckian limit breaking is associated with a fully quantum mechanical transport regime beyond the QP scattering paradigm. While the Planckian limit breaking has been typically associated with strange metals and other strongly correlated phases of matter [48–50], our results highlight that strong e -ph interactions can also lead to this quantum mechanical transport regime.

V. CONCLUSION

In summary, we developed a broadly applicable approach for computing charge transport in the large polaron regime in materials with intermediate e -ph coupling strength. Our calculations on SrTiO₃ unveil a transition from band-like transport of strongly weight-renormalized QPs at low temperature to an incoherent transport regime beyond the QP picture near room temperature. Our approach can shed new light on broad classes of materials with polaron effects, ranging from perovskites [51] and transition metal oxides [52, 53] to high- T_c superconductors [54, 55].

ACKNOWLEDGMENTS

J.-J.Z. has benefited from discussion with N.-E. Lee. This work was supported by the Joint Center for Artificial Photosynthesis, a DOE Energy Innovation Hub, supported through the Office of Science of the U.S. Department of Energy under Award No. DE-SC0004993. M.B. acknowledges support by the National Science Foundation under Grant No. ACI-1642443, which provided for code development, and Grant No. CAREER-1750613, which provided for theory and method development. This work was partially supported by the Air Force Office of Scientific Research through the Young Investigator Program, Grant FA9550-18-1-0280. This research used resources of the National Energy Research Scientific Computing Center, a DOE Office of Science User Facility supported by the Office of Science of the U.S. Department of Energy under Contract No. DE-AC02-05CH11231.

-
- [1] J. M. Ziman, *Electrons and Phonons: The Theory of Transport Phenomena in Solids* (Oxford University Press, New York, 2007).
- [2] H. Frhlich, *Adv. Phys.* **3**, 325 (1954).
- [3] T. Holstein, *Ann. Phys.* **8**, 343 (1959).
- [4] J. T. Devreese and A. S. Alexandrov, *Rep. Prog. Phys.* **72**, 066501 (2009).
- [5] D. Emin, *Polarons* (Cambridge University Press, 2012).
- [6] A. S. Mishchenko, N. Nagaosa, G. De Filippis, A. de Candia, and V. Cataudella, *Phys. Rev. Lett.* **114**, 146401 (2015).
- [7] J. L. M. van Mechelen, D. van der Marel, C. Grimaldi, A. B. Kuzmenko, N. P. Armitage, N. Reyren, H. Hagemann, and I. I. Mazin, *Phys. Rev. Lett.* **100**, 226403 (2008).
- [8] J. T. Devreese, S. N. Klimin, J. L. M. van Mechelen, and D. van der Marel, *Phys. Rev. B* **81**, 125119 (2010).
- [9] C. Chen, J. Avila, E. Frantzeskakis, A. Levy, and M. C. Asensio, *Nat. Commun.* **6**, 9585 (2015).
- [10] Z. Wang, S. McKeown Walker, A. Tamai, Y. Wang, Z. Ristic, F. Y. Bruno, A. de la Torre, S. Ricc, N. C. Plumb, M. Shi, *et al.*, *Nat. Mater.* **15**, 835 (2016).
- [11] H. P. R. Frederikse and W. R. Hosler, *Phys. Rev.* **161**, 822 (1967).
- [12] S. H. Wemple, M. DiDomenico, and A. Jayaraman, *Phys. Rev.* **180**, 547 (1969).
- [13] A. Verma, A. P. Kajdos, T. A. Cain, S. Stemmer, and D. Jena, *Phys. Rev. Lett.* **112**, 216601 (2014).
- [14] W. X. Zhou, J. Zhou, C. J. Li, S. W. Zeng, Z. Huang, *et al.*, *Phys. Rev. B* **94**, 195122 (2016).
- [15] T. A. Cain, A. P. Kajdos, and S. Stemmer, *Appl. Phys. Lett.* **102**, 182101 (2013).
- [16] X. Lin, C. W. Rischau, L. Buchauer, A. Jaoui, B. Fauqu, and K. Behnia, *npj Quantum Mater.* **2**, 41 (2017).
- [17] C. Collignon, X. Lin, C. W. Rischau, B. Fauqu, and K. Behnia, *Annu. Rev. Condens. Matter Phys.* **10**, 25 (2019).
- [18] E. Mikheev, B. Himmetoglu, A. P. Kajdos, P. Moetakef, T. A. Cain, C. G. V. d. Walle, and S. Stemmer, *Appl. Phys. Lett.* **106**, 062102 (2015).
- [19] N. E. Hussey, K. Takenaka, and H. Takagi, *Philos. Mag.* **84**, 2847 (2004).
- [20] J. T. Devreese, [arXiv:1611.06122 \[cond-mat\]](https://arxiv.org/abs/1611.06122) (2016).
- [21] M. Bernardi, *Eur. Phys. J. B* **89**, 239 (2016).
- [22] J. I. Mustafa, M. Bernardi, J. B. Neaton, and S. G. Louie, *Phys. Rev. B* **94**, 155105 (2016).
- [23] J.-J. Zhou and M. Bernardi, *Phys. Rev. B* **94**, 201201(R) (2016).
- [24] T.-H. Liu, J. Zhou, B. Liao, D. J. Singh, and G. Chen, *Phys. Rev. B* **95**, 075206 (2017).
- [25] J. Ma, A. S. Nissimagoudar, and W. Li, *Phys. Rev. B* **97**, 045201 (2018).
- [26] N.-E. Lee, J.-J. Zhou, L. A. Agapito, and M. Bernardi, *Phys. Rev. B* **97**, 115203 (2018).
- [27] J.-J. Zhou, O. Hellman, and M. Bernardi, *Phys. Rev. Lett.* **121**, 226603 (2018).
- [28] S. A. Hartnoll, *Nat. Phys.* **11**, 54 (2015).
- [29] A. Damascelli, Z. Hussain, and Z.-X. Shen, *Rev. Mod. Phys.* **75**, 473 (2003).
- [30] R. M. Martin, L. Reining, and D. M. Ceperley, *Interacting Electrons: Theory and Computational Approaches* (Cambridge University Press, 2016).
- [31] S. Baroni, S. de Gironcoli, A. Dal Corso, and P. Gianozzi, *Rev. Mod. Phys.* **73**, 515 (2001).
- [32] O. Hellman, I. A. Abrikosov, and S. I. Simak, *Phys. Rev. B* **84**, 180301(R) (2011).
- [33] J. J. Kas, J. J. Rehr, and L. Reining, *Phys. Rev. B* **90**, 085112 (2014).
- [34] J. J. Kas and J. J. Rehr, *Phys. Rev. Lett.* **119**, 176403 (2017).
- [35] L. Hedin, *J. Phys.: Condens. Matter* **11**, R489 (1999).
- [36] J. P. Nery, P. B. Allen, G. Antonius, L. Reining, A. Miglio, and X. Gonze, *Phys. Rev. B* **97**, 115145 (2018).
- [37] M. Berciu, *Phys. Rev. Lett.* **97**, 036402 (2006).
- [38] H. Hübener, U. De Giovannini, and A. Rubio, *Nano Lett.* **18**, 1535 (2018).
- [39] G. D. Mahan, *Many-Particle Physics*, 3rd ed. (Springer US, 2000).
- [40] J. S. Zhou, M. Gatti, J. J. Kas, J. J. Rehr, and L. Reining, *Phys. Rev. B* **97**, 035137 (2018).
- [41] A. S. Mishchenko, N. V. Prokofev, A. Sakamoto, and B. V. Svistunov, *Phys. Rev. B* **62**, 6317 (2000).
- [42] G. L. Goodvin and M. Berciu, *Europhys. Lett.* **92**, 37006 (2010).
- [43] E. N. Economou, “Electrical Conductivity and Greens Functions,” in *Greens Functions in Quantum Physics* (Springer, Berlin, Heidelberg, 2006) Chap. 8, pp. 173–198.
- [44] D. N. Basov, R. D. Averitt, D. van der Marel, M. Dressel, and K. Haule, *Rev. Mod. Phys.* **83**, 471 (2011).
- [45] P. B. Allen, *Phys. Rev. B* **92**, 054305 (2015).
- [46] X. Deng, A. Sternbach, K. Haule, D. N. Basov, and G. Kotliar, *Phys. Rev. Lett.* **113**, 246404 (2014).
- [47] A. S. Mishchenko, L. Pollet, N. V. Prokof’ev, A. Kumar, D. L. Maslov, and N. Nagaosa, *Phys. Rev. Lett.* **123**, 076601 (2019).
- [48] V. J. Emery and S. A. Kivelson, *Phys. Rev. Lett.* **74**, 3253 (1995).
- [49] O. Gunnarsson, M. Calandra, and J. E. Han, *Rev. Mod. Phys.* **75**, 1085 (2003).
- [50] J. A. N. Bruin, H. Sakai, R. S. Perry, and A. P. Mackenzie, *Science* **339**, 804 (2013).
- [51] K. Miyata, T. L. Atallah, and X.-Y. Zhu, *Sci. Adv.* **3**, e1701469 (2017).
- [52] S. Moser, L. Moreschini, J. Jaćimović, O. S. Barišić, H. Berger, A. Magrez, *et al.*, *Phys. Rev. Lett.* **110**, 196403 (2013).
- [53] C. Cancellieri, A. S. Mishchenko, U. Aschauer, A. Filippetti, C. Faber, O. S. Bari, V. A. Rogalev, T. Schmitt, N. Nagaosa, and V. N. Strocov, *Nat. Commun.* **7**, 10386 (2016).
- [54] A. Lanzara, P. Bogdanov, X. Zhou, S. Kellar, D. Feng, E. Lu, T. Yoshida, H. Eisaki, A. Fujimori, K. Kishio, *et al.*, *Nature* **412**, 510 (2001).
- [55] A. Legros, S. Benhabib, W. Tabis, F. Laliberté, M. Dion, M. Lizaire, B. Vignolle, D. Vignolles, H. Raffy, Z. Li, *et al.*, *Nat. Phys.* **15**, 142 (2019).